micromachines

MDPI

Communication

The Impact of Hydrogen on Mechanical Properties; A New In Situ Nanoindentation Testing Method

Christian Müller [1], Mohammad Zamanzade [1,2,*] and Christian Motz [1]

[1] Department of Materials Science and Methods, Saarland University, Bldg. D2.2, 66123 Saarbrücken, Germany; c.mueller@matsci.uni-saarland.de (C.M.); motz@matsci.uni-sb.de (C.M.)

[2] Mines Saint-Etienne, Univ Lyon, CNRS, UMR 5307LGF, Centre SMS, F-42023 Saint-Etienne, France

* Correspondence: mohammad.zamanzade@emse.fr; Tel.: +33-0-477420048

Received: 13 January 2019; Accepted: 6 February 2019; Published: 11 February 2019

Abstract: We have designed a new method for electrochemical hydrogen charging which allows us to charge very thin coarse-grained specimens from the bottom and perform nanomechanical testing on the top. As the average grain diameter is larger than the thickness of the sample, this setup allows us to efficiently evaluate the mechanical properties of multiple single crystals with similar electrochemical conditions. Another important advantage is that the top surface is not affected by corrosion by the electrolyte. The nanoindentation results show that hydrogen reduces the activation energy for homogenous dislocation nucleation by approximately 15–20% in a (001) grain. The elastic modulus also was observed to be reduced by the same amount. The hardness increased by approximately 4%, as determined by load-displacement curves and residual imprint analysis.

Keywords: nickel; nanoindentation; hardness; brittleness and ductility; hydrogen embrittlement

1. Introduction

Conventional mechanical testing methods have been used for quantitative studies of the influence of hydrogen on mechanical properties, e.g., yield stress, ultimate tensile stress and fracture strain [1]. However, these techniques are not very successful in obtaining mechanistic information because they simultaneously probe a large volume of the material and only provide an averaged result as if the volume were homogeneous. In fact, macroscopic samples contain inhomogeneities such as vacancies, dislocations and grain boundaries, which are known to play an important role in hydrogen embrittlement [2–4]. In contrast to macroscopic experiments, local testing methods enable us to decrease the probed volume of material, perform measurements for a quasi-homogeneous volume of material and hence decrease the possible sources of scattering in the results [5–7]. Additionally, as a result of the small probed volume, the hydrogen concentration can be assumed to be constant. In the past, we have used various local, in situ experimental techniques, such as electrochemical nanoindentation, in situ compression and bending of micro-pillars, to study the contribution of solute hydrogen on elastic properties, dislocation nucleation and hardness of alloys. These techniques enabled us to achieve an understanding of the mechanisms of hydrogen embrittlement (HE) for a material in a certain medium. Furthermore, we were able to rank the sensitivity of different alloys to hydrogen embrittlement in a specific medium irrespective of the impacts of grain boundaries, phase boundaries, pores, etc. [5–7].

However, there is still room for improvement to make electrochemical setups easier and experiments more reproducible. Our previous in situ nanoindentation approach comprised a layer of electrolyte on the specimen surface, which was penetrated by the tip during indentation. This had several disadvantages: (i) capillary forces acting on the tip; (ii) an inability to use the optical microscope of the machine for positioning; (iii) either an electrolyte flow causing vibrations or a static electrolyte

film, in which no chemical reaction products are washed away from the surface; (iv) corrosion of the tested surface and, accordingly, (v) limited time for hydrogen charging as well as mechanical testing. In this paper, a new testing setup for studying the impact of hydrogen on mechanical properties is introduced. With this method, hydrogen is provided at the bottom surface of a thin sample while nanoindentation is performed on the top surface. This method avoids most of the problems named above and also allows the analysis of previously unobtainable properties with respect to diffusion.

2. Experiments

Pure (99.9%) polycrystalline, square-shaped nickel specimens were milled from the back, heat-treated at 1240 °C for grain growth, ground in multiple steps, and finally electropolished with a solution of 1M sulfuric acid solved in methanol. These steps minimized the possible amount of residual stress and plastic deformation in the material, especially near the surface, where no sources for inhomogeneous dislocation nucleation were desired. The resulting specimen geometry had a thickness of approximately 200 µm in the region of interest (marked as the area with superimposed electron backscatter diffraction (EBSD) map in Figure 1), which was smaller than the average grain diameter (~500 µm). The sample was then glued to the dedicated cell made from polyvinyl chloride (PVC). The holes in the base plate of the cell allowed us to securely install it in the indenter, ensuring it was positioned identically before and after hydrogen permeation. The detailed specimen preparation and configuration of the electrochemical setup have been published elsewhere [8].

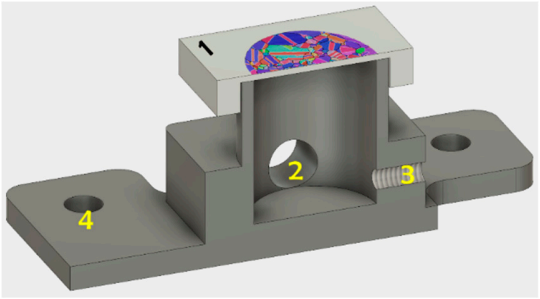

Figure 1. Cross section of specimen and electrochemical cell. (1) Nickel specimen, (2) electrolyte in-/output, (3) screw as counter electrode (4) holes for fixation in the nanoindenter.

The first electrochemical hydrogen charging step was carried out ex situ for two days with a constant current density of 14.5 A/m^2, applied by an IVIUM CompactStat (Ivium Technologies B.V., Eindhoven, The Netherlands). A 0.25 molar H_2SO_4 solution was used as the electrolyte, containing 5 g/L potassium iodide (KI) as hydrogen recombination poison. To remove hydrogen bubbles at the charging surface, the sample was inverted and the solution was steadily pumped in and out. The risk of outgassing was accounted for by charging in situ during measurements. For this purpose, a lower current density of 0.25 A/m^2 was applied and the flow rate of the pumped solution was decreased to avoid vibrations. Furthermore, a borate buffer solution (mixed using 1.24 g/L H_3BO_3 and 1.91 g/L $Na_2B_4O_7{\cdot}10H_2O$, also supplemented with 5 g/L KI) was used instead of sulfuric acid. However, the outgassing of hydrogen may also be considerably reduced by the existence of a homogeneous passive layer [8,9], which was measured to be approximately 10 nm, using a JEOL JEM-ARM200F transmission electron microscope (TEM).

As a proof of concept, a (001)-oriented grain was tested before and after hydrogen charging. Nanoindentation was performed with a Hysitron Triboindenter (Bruker Corporation, Billerica, MA, USA), equipped with Performech controller and a diamond Berkovich tip with a tip radius of approximately 400 nm. The applied indentation parameters are summarized in Table 1, where "fast" and "slow" corresponds to the loading rate.

Table 1. Nanoindentation parameters.

Measured Parameter	Max. Load	Load or Strain Rate	Type of Test	# of Indents
Pop-in slow	700 µN	50 µN·s^{-1}	Quasi static	60
Pop-in fast	700 µN	5000 µN·s^{-1}	Quasi static	60
Hardness fast	10 mN	0.5 s^{-1}	Quasi static	10
Hardness slow	10 mN	0.05 s^{-1}	Dynamic NanoDMAIII	10

3. Results and Discussions

We observed an elastic deformation of the thin membrane during nanoindentation despite the low applied forces. Quantitative analysis of the results was performed after precise evaluation of total system compliance, which can be interpreted as a series connection of three springs: (i) compliance of the machine frame, (ii) PVC cell and the glues used to install the sample, and (iii) the deflection of the thin nickel membrane. The first calibration was a standard calibration involving the indentation of a fused quartz reference with high forces. The second spring constant was evaluated by testing a bulky nickel sample installed on the same cell and attached with the same glue. To evaluate the third spring constant or the effect of the bending of the whole membrane on the nanoindentation curves, the continuous stiffness method (Hysitron NanoDMA measurement) was used. This technique measures the elastic modulus at every indentation depth by continuously oscillating the tip. On a reference specimen, we verified that the modulus of the nickel bulk is independent of depth. Hence, the internal compliance value in all other data files were modified until their NanoDMA results also met this requirement.

Figure 2 shows load-displacement curves before and after charging. The pop-in or displacement burst phenomenon was related to the nucleation of dislocations around maximum shear stress under the tip [10]. The probability of the pop-in event did not change after hydrogen charging (in both cases more than 95%). The few curves in which no distinct pop-in could be detected are not displayed. A 15% reduction of average $P_{\mathrm{pop-in}}$ values was determined to be attributable to hydrogen charging as well as a slight increase in scattering. The scattering in $P_{\mathrm{pop-in}}$ is a common observation in nanoindentation experiments, originating from the thermal activation of homogenous dislocation nucleation [11,12].

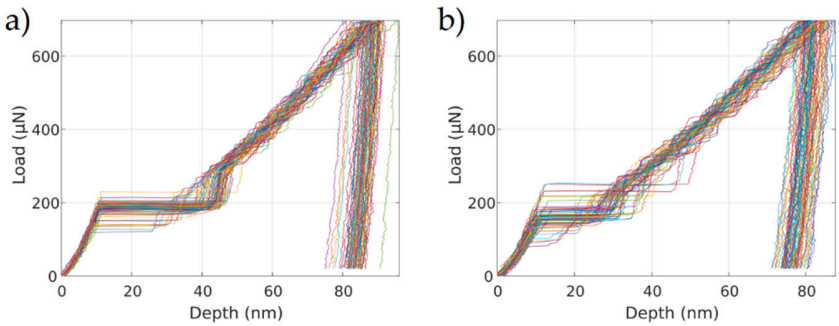

Figure 2. Load-displacement curves recorded with the fast loading rate (**a**) before charging and (**b**) after charging with hydrogen. Curves in which no pop-in could be detected were filtered.

Results indicate that the critical energy needed for dislocation nucleation was decreased, which agrees with previous studies [5,7,13]. Because of the slight reduction of the average values of pop-in load and because the population of the pop-in event did not change after charging, we can assume that the dislocation nucleation was homogeneous, and the observed behavior could be related to the debonding effect of hydrogen, known as hydrogen-enhanced decohesion (HEDE).

Another consequence of decohesion is the reduction of the elastic modulus, which was noticeable as a reduction of the slope in the Hertzian regimes, where the curves follow the equation [14]:

$$P = \frac{4}{3} E_r \sqrt{R} \times h^{3/2} \quad (1)$$

in which E_r is the reduced elastic modulus, R is the tip radius, P. is the applied load, and h the indentation depth. The load-displacement ($P - h$) data before the pop-in can be fitted to this equation with a fit parameter proportional to E_r. To visualize the differences and make them independent of R, a cumulative distribution of relative elastic moduli E_r / E_0 is plotted in Figure 3a, where E_0 is the average value before hydrogen charging. The reduction of reduced elastic modulus according to this analysis is approximately $17 \pm 10\%$, from 206 ± 20 GPa to 171 ± 17 GPa. Both individual values are in a realistic range for nickel. The reliability of each data point obtained by curve fitting and the deviation between individual points account for the uncertainty of this result. A more conventional method to determine Young's modulus in nanoindentation experiments is to fit the unloading segment with the model introduced by Oliver and Pharr [15]. Using this approach for our measurements, the moduli before and after charging were both approximately 200 GPa and were well inside the statistical error interval of each other.

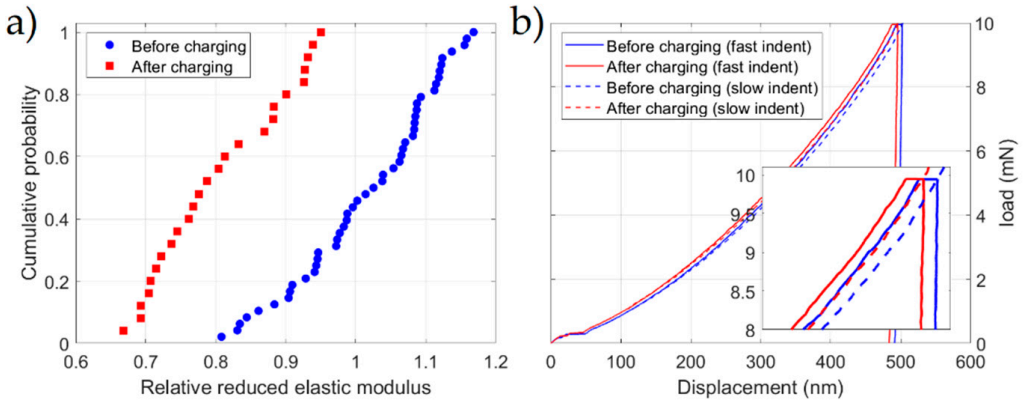

Figure 3. (**a**) Plot of reduced elastic modulus determined from Hertzian loading. (**b**) Load-displacement data of hardness measurements (averaged across 10 indents).

The occurrence of a measurable difference in Young's moduli due to hydrogen is controversial. For example, Lawrence et al. determined a comparable reduction by about 22% in nanoindentation experiments on nickel with the conventional Oliver-Pharr method [16]. In other studies, the difference was much smaller or even negligible, e.g., in molecular dynamics simulations of hydrogen in nickel [17]. Nevertheless, the analysis of elastic moduli is very much possible in our setup after the previously mentioned compliance correction.

Using the reduction of both $P_{\mathrm{pop-in}}$ and E_r, we can also calculate the reduction of the shear stress necessary for dislocation nucleation. According to the Hertzian model, the maximum shear stress under the tip is given by:

$$\tau_{\max} = 0.31 \times \left(\frac{6 P {E_r}^2}{\pi^3 R^2} \right)^{1/3} \tag{2}$$

in which both P and E_r are reduced by 15–17%, so the stress decreases by the same amount. The calculated values of approximately 5–7 GPa are close to the expected theoretical shear strength of nickel [18], which confirms that the cause of the pop-in was indeed homogenous dislocation nucleation.

Figure 3b shows the *P-h* curves performed to study the impacts of strain rates and dissolved hydrogen on the plastic behavior of Ni. Each curve is an average of ten indents, which was calculated and plotted. Similar to other solute atoms, hydrogen can contribute to the pinning of dislocations by forming Cottrell atmospheres around dislocation cores [19,20]. The resulting reduction of dislocation mobility becomes clear if we compare the hardness before and after hydrogen charging. Measurements after hydrogen charging systematically show a decreased indentation depth at the maximum load. Increasing the loading rate also results in a smaller depth and therefore higher hardness, but this effect appears to be independent of hydrogen concentration. After measuring the projected area of the residual imprint of every indent, we determined a 4.3% increase in hardness due to hydrogen

charging. Our results indicate that the application of various strain rates does not change this pining effect. Accordingly, the dislocations are constantly aged to saturation at room temperature at both tested strain rates. This means that when a dislocation escapes from a pinning point, the hydrogen diffusion is fast enough (relative to the dislocation velocity) to immediately follow and pin it again.

Another observation that reinforces the proposition of reduced dislocation mobility is a substantial reduction of pop-in width (also called excursion length) after hydrogen charging. As Figure 4 shows, a pop-in that happened at the same load P would, on average, cause a much smaller excursion length. This is attributable to the dislocations which show a drag force caused by hydrogen, decelerating the tip so that it stops earlier. Although excursion length is often assumed to solely represent the number of nucleated dislocations [21], we believe that the gliding of dislocations plays an important role in the measured pop-in width. Therefore, although hydrogen can ease the nucleation of dislocations, the reduction of the slope of the curves in Figure 4 after hydrogen charging could be related to the sessile behavior of dislocations.

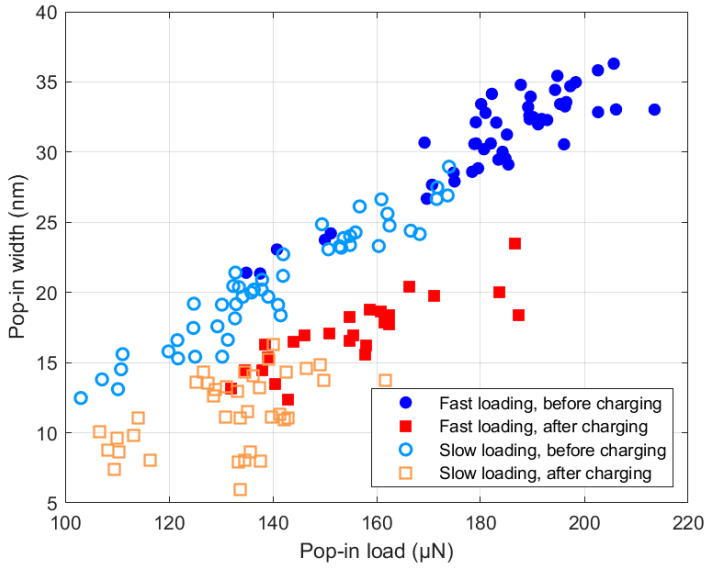

Figure 4. The impact of loading rate and hydrogen on the pop-in width and pop-in load.

4. Conclusions

The increase in hardness indicates a decreased mobility of dislocations due to the solute drag effect of hydrogen. However, hydrogen charging reduces the elastic modulus and the pop-in load and, accordingly, facilitates the formation of dislocations. The tested specimen geometry and charging conditions have proven to be successful and may be able to further analyze the influences of grain orientations and grain boundaries resulting from the testing of a thin layer charged from the back. The concept is promising for future research on diffusion coupled with changes in the mechanical properties of a variety of conductive materials.

One disadvantage introduced by the proposed setup is the consequence of the thin specimen geometry. The coarse-grained nickel layer is prone to deformation. Although its influence could be easily eliminated from nanoindentation curves, it leads to a long preparation procedure in which care must be taken in every step. Some of the electrochemical uncertainties also remain: The bottom of the sample may still be exposed to corrosion and the local hydrogen concentration at a certain point on the top can depend on inhomogeneities through which the hydrogen has to diffuse. In combination with potential discrepancies in delays between ex situ and in situ charging (and therefore outgassing), this remains a limitation on the quantitative reproducibility of specific results.

Author Contributions: Conceptualization, M.Z.; Methodology, M.Z. and C.M. (Christian Müller); Software, C.M. (Christian Müller); Validation, M.Z., C.M. (Christian Müller) and C.M. (Christian Motz); Formal Analysis, C.M. (Christian Motz); Investigation, M.Z. and C.M. (Christian Motz); Resources, M.Z., C.M. (Christian Müller) and C.M. (Christian Motz); Data Curation, C.M. (Christian Müller); Writing-Original Draft Preparation, C.M. (Christian Müller) and M.Z.; Writing-Review & Editing, C.M. (Christian Motz); Visualization, C.M. (Christian Müller); Supervision, C.M. (Christian Motz); Project Administration, M.Z., C.M. (Christian Müller) and C.M. (Christian Motz); Funding Acquisition, M.Z.

Funding: This research was funded by the Deutsche Forschungsgemeinschaft (DFG) grant number ZA 986/1-1.

Acknowledgments: Workshop manager Stefan Schmitz and Peter Limbach, TEM operator Jörg Schmauch, proof reader Isabelle Wagner.

Conflicts of Interest: The authors declare no conflict of interest.

References

1. Gangloff, R.P.; Somerday, B.P. *Gaseous Hydrogen Embrittlement of Materials in Energy Technologies: Mechanisms, Modelling and Future Developments*; Elsevier: Amsterdam, The Netherlands, 2012; ISBN 0857095374.
2. Angelo, J.E.; Moody, N.R.; Baskes, M.I. Trapping of hydrogen to lattice defects in nickel. *Model. Simul. Mater. Sci. Eng.* **1995**, *3*, 289–307. [CrossRef]
3. Besenbacher, F.; Myers, S.M.; Nørskov, J.K. Interaction of hydrogen with defects in metals. *Nucl. Instruments Methods Phys. Res. Sect. B Beam Interact. Mater. Atoms* **1985**, *7*, 55–66. [CrossRef]
4. Myers, S.M.; Baskes, M.I.; Birnbaum, H.K.; Corbett, J.W.; DeLeo, G.G.; Estreicher, S.K.; Haller, E.E.; Jena, P.; Johnson, N.M.; Kirchheim, R. Hydrogen interactions with defects in crystalline solids. *Rev. Mod. Phys.* **1992**, *64*, 559. [CrossRef]
5. Barnoush, A.; Vehoff, H. Recent developments in the study of hydrogen embrittlement: Hydrogen effect on dislocation nucleation. *Acta Mater.* **2010**, *58*, 5274–5285. [CrossRef]
6. Zamanzade, M.; Barnoush, A. An overview of the hydrogen embrittlement of iron aluminides. *Procedia Mater. Sci.* **2014**, *3*, 2016–2023. [CrossRef]
7. Barnoush, A.; Zamanzade, M. Effect of substitutional solid solution on dislocation nucleation in Fe_3Al intermetallic alloys. *Philos. Mag.* **2012**, *92*, 3257–3268. [CrossRef]
8. Zamanzade, M.; Müller, C.; Velayarce, J.R.; Motz, C. Susceptibility of different crystal orientations and grain boundaries of polycrystalline Ni to hydrogen blister formation. *Int. J. Hydrogen Energy* **2019**. Acccepted for publication.
9. Condon, J.B.; Schober, T. Hydrogen bubbles in metals. *J. Nucl. Mater.* **1993**, *207*, 1–24. [CrossRef]
10. Wen, M.; Zhang, L.; An, B.; Fukuyama, S.; Yokogawa, K. Hydrogen-enhanced dislocation activity and vacancy formation during nanoindentation of nickel. *Phys. Rev. B* **2009**, *80*, 094113. [CrossRef]
11. Gao, X. Displacement burst and hydrogen effect during loading and holding in nanoindentation of an iron single crystal. *Scr. Mater.* **2005**, *53*, 1315–1320. [CrossRef]
12. Zamanzade, M.; Hasemann, G.; Motz, C.; Krüger, M.; Barnoush, A. Vacancy effects on the mechanical behavior of B2-FeAl intermetallics. *Mater. Sci. Eng. A* **2018**, *712*, 88–96. [CrossRef]
13. Zamanzade, M.; Vehoff, H.; Barnoush, A. Cr effect on hydrogen embrittlement of Fe_3Al-based iron aluminide intermetallics: Surface or bulk effect. *Acta Mater.* **2014**, *69*, 210–233. [CrossRef]
14. Hertz, H. On the contact of elastic solids. *J. Reine Angew Math.* **1881**, *92*, 156–171.
15. Oliver, W.C.; Pharr, G.M. An improved technique for determining hardness and elastic modulus using load and displacement sensing indentation experiments. *J. Mater. Res.* **1992**, *7*, 1564–1583. [CrossRef]
16. Lawrence, S.K.; Somerday, B.P.; Karnesky, R.A. Elastic property dependence on mobile and trapped hydrogen in Ni-201. *Jom* **2017**, *69*, 45–50. [CrossRef]
17. Wen, M.; Barnoush, A.; Yokogawa, K. Calculation of all cubic single-crystal elastic constants from single atomistic simulation: Hydrogen effect and elastic constants of nickel. *Comput. Phys. Commun.* **2011**, *182*, 1621–1625. [CrossRef]
18. Černý, M. *Theoretical Strength and Stability of Crystals from First Principles*; VUTIUM: Brno, Czech Republic, 2008.
19. Cottrell, A.H.; Jaswon, M.A. Distribution of solute atoms round a slow dislocation. *Proc. R. Soc. Lond. A.* **1949**, *199*, 104–114.

20. Delafosse, D. *Hydrogen Effects on the Plasticity of Face Centred Cubic (fcc) Crystals*; Woodhead Publishing: Sawston, Cambridge, UK, 2012; ISBN 9780857095367.
21. Bahr, D.F.; Kramer, D.E.; Gerberich, W.W. Non-linear deformation mechanisms during nanoindentation. *Acta Mater.* **1998**, *46*, 3605–3617. [CrossRef]